NANO LETTERS

2006
Vol. 6, No. 1
89−95

Salt Dependence of Ion Transport and DNA Translocation through Solid-State Nanopores

Ralph M. M. Smeets, Ulrich F. Keyser, Diego Krapf, Meng-Yue Wu, Nynke H. Dekker, and Cees Dekker*

Kavli Institute of Nanoscience, Delft University of Technology, Lorentzweg 1, 2628 CJ Delft, The Netherlands

Received October 25, 2005; Revised Manuscript Received November 15, 2005

ABSTRACT

We report experimental measurements of the salt dependence of ion transport and DNA translocation through solid-state nanopores. The ionic conductance shows a three-order-of-magnitude decrease with decreasing salt concentrations from 1 M to 1 μM, strongly deviating from bulk linear behavior. The data are described by a model that accounts for a salt-dependent surface charge of the pore. Subsequently, we measure translocation of 16.5-μm-long dsDNA for 50 mM to 1 M salt concentrations. DNA translocation is shown to result in either a decrease ([KCl] > 0.4 M) or increase of the ionic current ([KCl] < 0.4 M). The data are described by a model where current decreases result from the partial blocking of the pore and current increases are attributed to motion of the counterions that screen the charge of the DNA backbone. We demonstrate that the two competing effects cancel at a KCl concentration of 370 ± 40 mM.

Introduction. Nanometer-sized pores can serve as single-molecule sensors for the detection and analysis of biopolymers. Sensing of single-stranded DNA (ssDNA) and ssRNA at the single-molecule level was first demonstrated using the protein pore α-hemolysin (narrowest constriction of 14 Å).[1,2] This protein-pore-based sensor was able to discriminate between different nucleic acid molecules,[3,4] detect single-nucleotide differences,[5] and characterize the hybridization of individual DNA strands.[6] Fabricated solid-state nanopores[7,8] offer advantages over protein-based pores, such as size control, increased chemical, electrical, mechanical, and thermal stability, and the potential of device integration. Solid-state pores have been used to map the three-dimensional intensity profile of a laser,[9] detect DNA contour lengths,[10] DNA hybridization,[11] DNA folding,[12,13] and the drag[10] on individual DNA molecules. Narrow (1-nm diameter) solid-state pores were also used to filter ssDNA from a solution containing ssDNA and dsDNA.[14]

The physical detection principle of the nanopore sensor is similar to that of Coulter counters, which are typically used for the detection of micrometer-sized particles. The introduction of such a particle into a small capillary results in partial blocking of the ionic current. As particles are driven through the opening, spike-like decreases in the current can be recorded, which are related to the volume of the particles.[15] Nanopore diameters are a thousand times smaller than those of typical Coulter counters and, consequently, nanopores are capable of detecting objects on the molecular scale. However, at these length scales surface effects may also play a role in the current signal during translocation. The influence of surface charges on ionic transport was reported recently in nanochannels[16−18] and in small-diameter synthetic nanopores.[19−20] DNA translocations through nanopores[21] and nanochannels[22] at isolated low salt concentrations were recently shown to result in current *enhancements* rather than current decreases.

In this letter, we study the salt dependence of ion transport and dsDNA translocation through solid-state nanopores over a wide range of concentrations. We present ion transport measurements through nanopores over salt concentrations spanning 6 orders of magnitude. The results are compared to models of bulk behavior and constant-surface-charge conductance, which both fail to describe the data. We introduce a simple model that additionally accounts for the salt-dependent charging of SiO_2 and obtain a good description of the data. Furthermore, we present DNA translocations through nanopores over a range of salt concentrations. DNA translocation results in either a decrease or increase of the ionic current. Two competing effects are identified for the current change. We demonstrate the existence of a cross-over point at which DNA translocation causes no current change. Together, the experiments yield a complete picture of the salt dependence of DNA translocation through nanopores.

* Corresponding author. Fax: +31-15-2781202. E-mail: dekker@mb.tn.tudelft.nl.

10.1021/nl052107w CCC: $33.50
Published on Web 12/13/2005

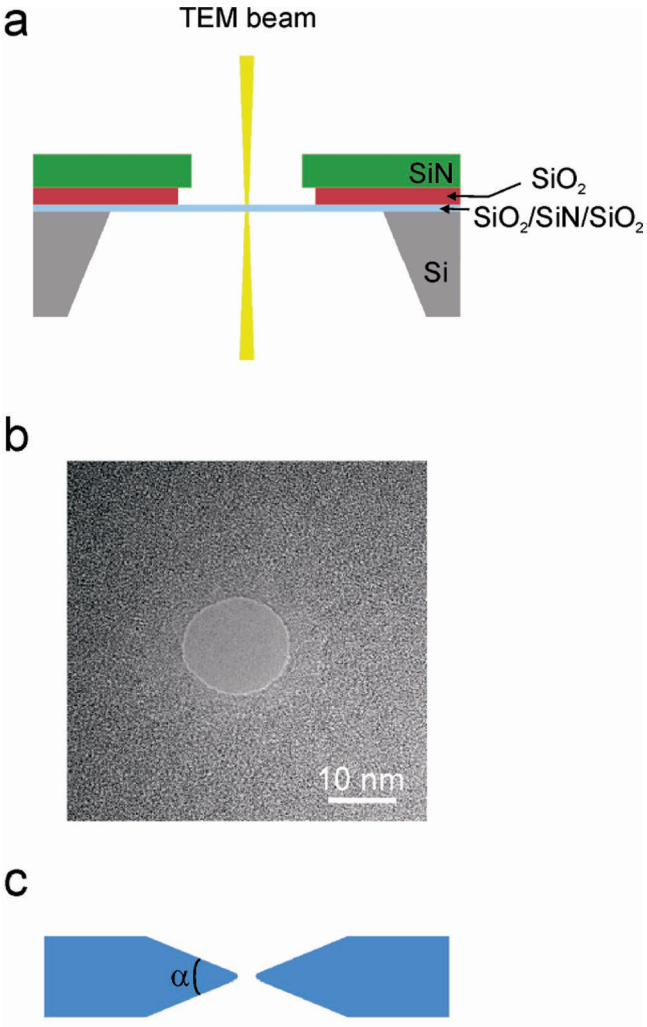

Figure 1. Nanopore fabrication and layout. (a) Schematic of the use of a tightly focused electron beam (yellow) on a thin fabricated membrane, resulting in the creation of a nanopore. The material composition of the different layers is indicated in the figure. (b) Transmission electron micrograph of a nanopore (diameter 12 nm) immediately after its formation by the intense electron beam. (c). Schematic cross-section of a fabricated nanopore as inferred from EELS measurements. Only the thin silicon oxide/silicon nitride/silicon oxide membrane is shown. The drilling process results in the removal of material in a broad area around the opening. The indicated angle, α, is approximately 45 degrees.

Fabrication of Nanopores and Experimental Setup. A three-layer structure of 20-nm silicon nitride, 200-nm silicon dioxide, and 500-nm silicon nitride was deposited by low-pressure chemical-vapor deposition (LPCVD) on silicon (100) wafers. A thin free-standing membrane of silicon nitride was fabricated by opening a window in the unpolished side of the wafer using electron-beam lithography, followed by reactive ion etching (RIE, CHF_3/O_2) to remove the deposited layers, after which a KOH wet etch removed the silicon. Next, a window was opened on the polished top side of the wafer, again using electron-beam lithography. The top silicon nitride and silicon dioxide layers were removed with an RIE (CHF_3/O_2) and a buffered HF etch, respectively. The resulting free-standing silicon nitride membrane was covered with a thin layer of sputtered silicon oxide (~20 nm) on both sides. This resulted in a hydrophilic membrane surface, while the structure still had the ease of fabrication and good insulation properties of a silicon nitride membrane.

Finally, the sample was placed in a transmission electron microscope (TEM) operated at 200 or 300 kV. The use of a tightly focused electron beam (2−10 nm full width at half-maximum, 10^8-10^9e/nm^{2}s beam intensity) on the membrane resulted in the sputtering of material and hence the creation of a nanopore, as depicted schematically in Figure 1a. The size of the nanopore could be tuned by using a defocused electron beam with lower intensity (10^6-10^7e/nm^{2}s), which prevents sputtering but does enable surface-tension-driven transport of material.[8] The produced nanopores were imaged directly in the TEM (Figure 1b). The diameter of the pores used in these experiments was approximately 10 nm. Information about the three-dimensional geometry was obtained by mapping the thickness variation around the opening using electron energy-loss spectroscopy (EELS).[23] The EELS results indicated that the length of the narrowest constriction of the nanopore is much smaller than the 60-nm thickness of the membrane, as depicted schematically in Figure 1c.

Prior to inserting the nanopores in the experimental setup for measuring ionic current through the pore, both sides of the sample were subjected to an oxygen plasma for about 15 s. This process removed any organic contaminants and resulted in the oxidation of the surface (SiO_2), which enhanced the wettability properties of the nanopores significantly. Next, the patterned chip was placed between two liquid compartments of a flow cell. One compartment was formed by adhering a patterned poly(dimethylsiloxane) (PDMS) layer to a glass slide, forming a channel connecting the sample to fluid inlet and outlet. The other compartment consisted of a channel constructed in a poly(methyl methacrylate) (Perspex) block, which was sealed against the sample with an O-ring. The nanopore formed the only connection between the two compartments. Ag/AgCl electrodes were placed at the outlets of both channels and connected to an amplifier (Axopatch 200B, Axon Instruments, USA). Solutions could be exchanged easily within each compartment by flowing liquid through the channels. Salt solutions were prepared by adding 18 MΩcm Milli-Q filtered water (Millipore) to a stock solution of 1 M potassium chloride with 20 mM TRIS−HCl buffer at pH = 7.5. Unmethylated 48.5 kbp double-stranded λ-DNA (Promega, Benelux) was used in the translocation studies.

The value of the nanopore conductance at various salt concentrations was obtained by sweeping the voltage over a range of ±200 mV at a scan rate of approximately 6 mV/s. For DNA translocation, a constant voltage of 120 mV was applied. When DNA was introduced into one of the two compartments, spike-like changes were observed in the current. This current signal was digitized at 200 kHz (Axon 1322A digitizer, Axon Instruments) and low-pass filtered with a cutoff frequency of 10 kHz. When necessary, the data was subjected to an additional external filter of 5 kHz to increase the signal-to-noise ratio. The event-fitting algorithm used to analyze and label the translocation events was similar to the one described by Storm et al.[13] We modified the

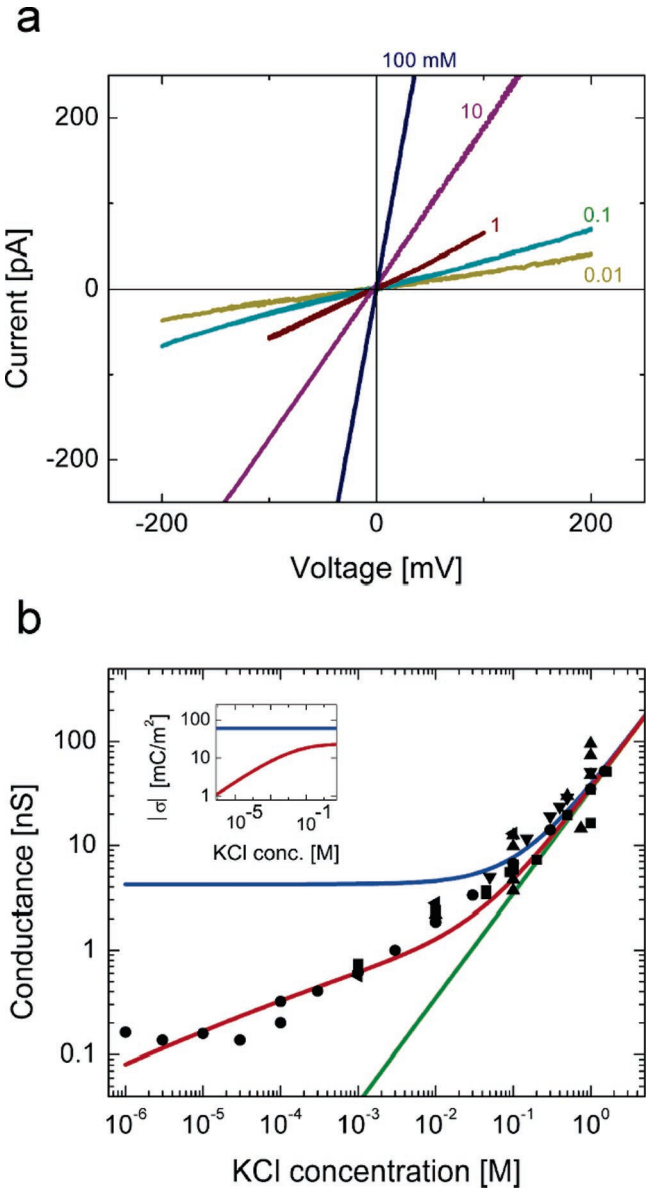

Figure 2. Salt concentration dependence of nanopore conductance. (a) Current−voltage characteristics for a single 10.2-nm-diameter pore at KCl concentrations of 0.01, 0.1, 1, 10, and 100 mM, as indicated. All curves show a linear $I-V$ dependence. (b) Conductance values of 10 individual pores measured for KCl concentrations from 1 μM to 1 M. Each individual pore has its own symbol. The black upright triangles represent individual pores that were used at a single salt concentration. All of the pores used have diameters of 10 ± 2 nm. The green, blue, and red lines show the results of calculations as predicted by bulk behavior, a model for constant surface charge, and a model for a variable surface charge, respectively (see text). For the calculations, a 10-nm-diameter and 34-nm-long cylindrical pore was assumed. The inset shows the values of the surface-charge density vs salt concentrations on a log−log scale, for both the constant surface charge model (blue, σ = 60 mC/m^2) and the variable-charge model (red, parameters are given in ref 36).

procedure slightly to determine the open-pore current by averaging the current before and after the event for approximately 2 ms. Furthermore, in the present algorithm the events start and end upon reaching the baseline current value. We have discarded levels lasting shorter then 70 μs (210 μs for the events that were additionally filtered at 5 kHz).

Experimental Results. *Salt Dependence of the Nanopore Conductance.* Figure 2a shows an example of current−voltage ($I-V$) measurements of a single 10-nm pore at five different potassium chloride concentrations. In all experiments, the $I-V$ curves display a linear relationship. Fits to the data yield the value of the pore conductance. Its value clearly decreases as the potassium chloride concentration is lowered. The conductance of 10 individual nanopores as a function of the potassium chloride concentration is shown in Figure 2b. As the salt concentration is varied over 6 orders of magnitude, the conductance is found to decrease by a factor of ∼1000. In the high-salt regime ([KCl] ≥ 100 mM), the conductivity of the nanopores is comparable to the bulk conductivity of KCl. In this regime, the conductance agrees with a linear dependence on potassium chloride concentration as expected for bulk liquid. The green straight line indicates the expected bulk behavior for a cylindrical nanopore of 10 nm in diameter and 34 nm in length. These pore dimensions are used in all calculations; the diameter of the cylindrical model pore is inferred from the TEM images, and the choice for the length is justified below. In the low-salt regime ([KCl] < 100 mM), we measure a much larger conductance than expected from bulk behavior. The data show a gradual decrease in conductance as the potassium chloride concentration is lowered, all the way down to 1 μM.

DNA Translocation through Nanopores at Various Salt Concentrations. We now turn to the spike-like changes in the conductance that are observed following the introduction of DNA molecules (Figure 3). The sign of the current changes is found to depend on the salinity of the solution. Figure 3a shows the data of three individual DNA translocation events at a high KCl concentration (500 mM, black). Spike-like decreases in the ionic current are observed that are quantified using an event-fitting algorithm (red). The current before and after the decrease equals the ionic current in the absence of DNA in the pore. As the three traces demonstrate, not all of the DNA translocations show the same magnitude of current decrease. The first and the last trace show a current decrease that differs by approximately a factor of 2. The second trace shows two different current levels, each of which is similar to the levels in the two other traces. In this particular case, a larger current blockade is followed by a smaller one. Following the nomenclature of ref 13, we call this a 21 event, whereas the events on the left and right of Figure 3a are called 1 and 2 events, respectively. It is shown that these different types of events result from DNA molecules traversing the pore in different folding conformations where a 1 event is caused by an unfolded DNA molecule and a 21 event is caused by a DNA that enters in a folded state and exits with its unfolded tail.[12,13] Consequently, the smaller current amplitude blockades exhibit longer translocation times (Figure 3a).

We next monitor DNA translocation in the same pore (d_{pore} = 10.2 nm) but at a lower KCl concentration of 150 mM. Surprisingly, spike-like current *increases* are recorded at this low salt concentration (Figure 3b). The magnitude of the current increases could again differ by approximately a factor of 2, as shown by the first and last trace. The second trace

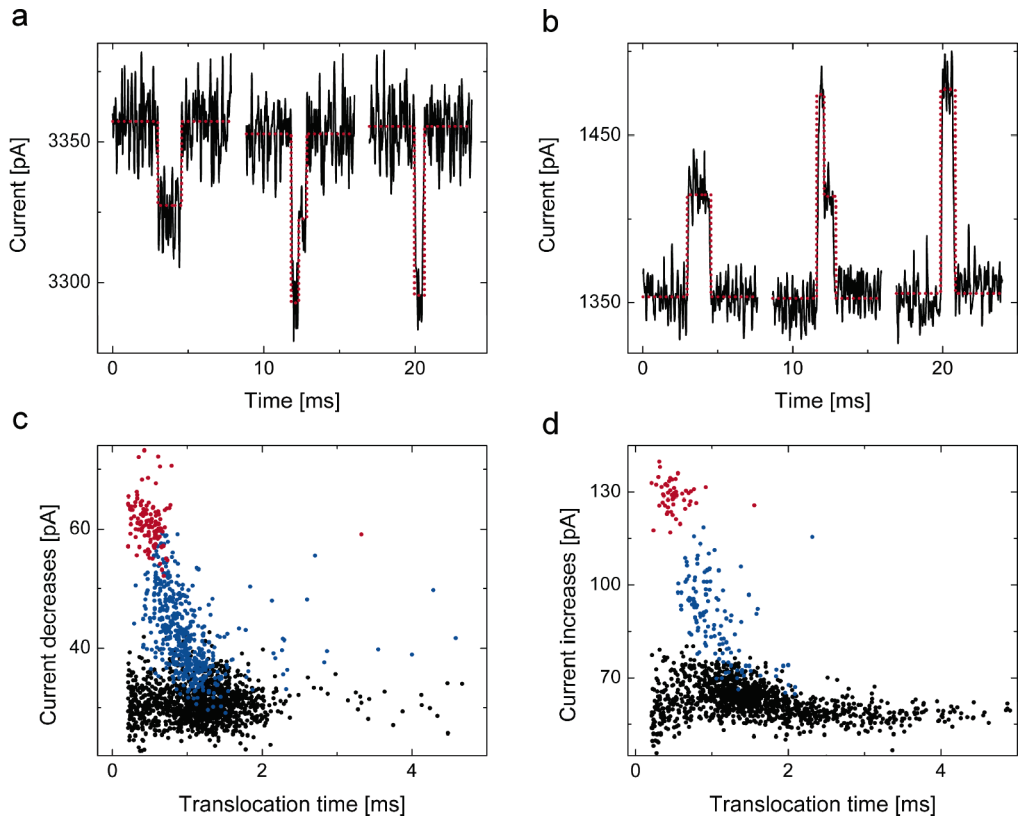

Figure 3. DNA translocation resulting in current *decreases* at 500 mM, and current *enhancements* at 150 mM KCl. (a) Examples of three individual DNA translocation events at KCl concentrations of 500 mM and (b) 150 mM. The data in a and b were measured using the same pore of 10.2-nm-diameter. Data shown in black was additionally filtered at 5 kHz. The red dotted lines display the result of the event-fitting algorithm. The traces displayed show subsequent translocation of unfolded, partially folded, and fully folded DNA molecules from left to right, respectively. (c) Event scatter diagram of the amplitude of the current change vs translocation time for the salt concentration of 500 mM. (d) Same for 150 mM. Color coding represents translocation of unfolded (black), partially folded (blue), and fully folded (red) DNA molecules.

displays two levels of current increases, in this case a large increase followed by a smaller one. We again categorize the traces as 1, 21, and 2 events. Again, smaller current amplitude increases are found to correlate with longer translocation times.

We now compare these events at the two different potassium chloride concentrations by analyzing scatter plots of the change in current versus the time duration of the event. They are presented in Figure 3c and d for salt concentrations of 500 mM and 150 mM, respectively. The color coding reflects the 1, 21, and 2 events as identified above. For a KCl concentration of 500 mM (Figure 3c), the amplitude of the current decreases range from approximately 30 to 60 pA from the 1 (black) to 2 events (red). The current increases at a KCl concentration of 150 mM range from approximately 60 to 130 pA. In both cases, the level of current change for the 2 events is approximately twice as large as that of the 1 events. The most probable translocation times for the 1 and 2 events are, respectively, 1.2 ± 0.1 ms and 0.48 ± 0.05 ms for a KCl concentration of 500 mM and 1.4 ± 0.1 ms and 0.45 ± 0.04 ms for 150 mM.[24] Clearly, the characteristics of the spike-like ionic current enhancements are strikingly similar to those of the current blockades, with the obvious exception that the sign of the current change is reversed. From the similarities between the distinct current levels and the translocation times, we infer that the recorded current enhancements are caused by DNA translocation through the nanopore.

We subsequently measure translocation events over a range of salt concentrations (1 M down to 50 mM, Figure 4a). Attemps to measure DNA translocation at 1 mM and 10 mM KCl concentrations did not yield any translocation events. For simplicity, only unfolded type-1 DNA translocation events are considered in the analysis. The conductance changes, ΔG, due to DNA translocation are found to change gradually from blockades to enhancements as the KCl concentration is lowered from 1 M.[25] Moreover, the conductance change appears to be linearly proportional (red line) to the concentration of ions in the bulk solution. The linear fit yields a crossover point, at which current decreases change to current enhancements, at a KCl concentration of 370 ± 40 mM.

In principle, the conductance change, ΔG, depends on the length of the nanopore. Because of potential geometrical variations from pore to pore, one might argue that it is more reasonable to consider the *relative* change in conductance, $\Delta G/G$, because its value no longer depends on the length of the nanopore but only on its diameter, which is known from TEM imaging. In Figure 4b, we have plotted the relative conductance change as a function of potassium chloride

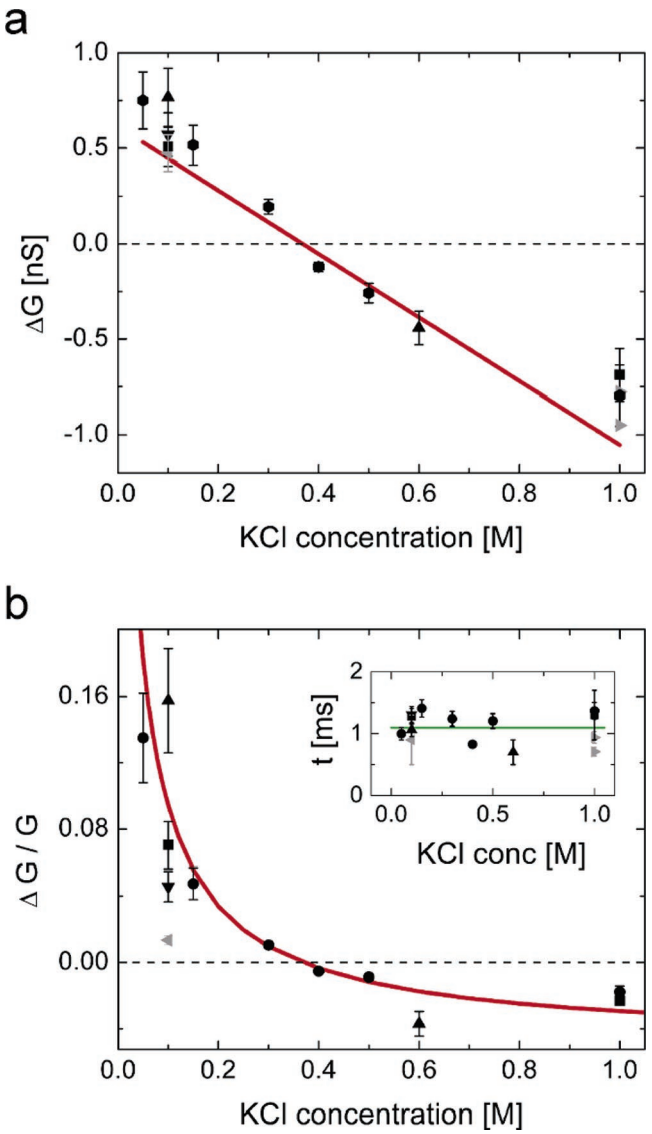

Figure 4. Conductance changes (a) and relative conductance changes (b) due to DNA translocation for KCl concentrations between 50 mM and 1 M. Only unfolded (type-1) DNA translocations are analyzed. Each symbol represents an individual pore of diameter 10 ± 2 nm except for the gray right (15 nm) and left (21 nm) pointing triangles. The red line in a represents a linear fit to the data. The red line in b represents calculated values upon taking a changing surface charge into account and using the values obtained from the fit in a (see text). The inset in b shows the DNA translocation time as a function of KCl concentration.

concentration. Again, a transition from a decreasing to an increasing change in conductance is observed. The relative change in conductance is much higher in the low-salt regime, which is caused by the lower conductance, G, of the nanopore. The values of $\Delta G/G$ show considerable scatter at a KCl concentration of 0.1 M, whereas the values of ΔG (Figure 4a) are similar. This scatter is caused by variations in the conductance, G, for different nanopores of similar size (Figure 2b).

The most probable DNA translocation time as a function of potassium chloride concentration is shown in the inset of Figure 4b. Within the experimental error, the translocation time appears to be constant over the KCl concentrations probed. Because the translocation time is directly related to the electrophoretic mobility of the DNA, the result suggests that the electrophoretic mobility of DNA is constant for KCl concentrations from 50 mM to 1 M.

Modeling and Discussion. *Salt Dependence of the Nanopore Conductance.* Because of the high surface-to-volume ratio in nanopores, surfaces potentially have a large effect on the conductance at lower salt concentrations. We now discuss how the nanopore conductance is influenced by surface charges in the pore. At high salt concentrations, we expect charge carriers in the solution to dominate the ionic current. The conductance should then scale linearly with the number of charge carriers, as observed experimentally (Figure 2b). The negative surface charge of the SiO_2 nanopore is screened by mobile K^+ counterions that contribute to the overall ionic current. The total current through the nanopore is therefore equal to the sum of the contributions of the bulk concentration of ions in solution and the counterions shielding the surface charge. The conductance, G, can be written as

$$G = \frac{\pi}{4}\frac{d_{\text{pore}}^2}{L_{\text{pore}}}\left((\mu_{\text{K}} + \mu_{\text{Cl}})n_{\text{KCl}}\, e + \mu_{\text{K}}\frac{4\sigma}{d_{\text{pore}}}\right) \qquad (1)$$

where d_{pore} represents the diameter, L_{pore} is the length of a cylindrical nanopore, n_{KCl} is the number density of potassium or chloride ions, e is the elementary charge, σ is the surface-charge density in the nanopore, and μ_{K} and μ_{Cl} are the electrophoretic mobilities of potassium and chloride ions, respectively. We use values of $\mu_{\text{K}} = 7.616 \times 10^{-8}$ m^2/Vs and $\mu_{\text{Cl}} = 7.909 \times 10^{-8}$ m^2/Vs.[26] The first term in eq 1 represents the bulk conductance, and the surface charge contribution to the conductance in the nanopore is given by the second term. At KCl densities higher than $n_{\text{KCl}} \gg 2\sigma/d_{\text{pore}}\, e$, the first term in the formula dominates the conductance and bulk behavior is observed. Deviations from bulk behavior start to occur when the first and the second term in eq 1 are comparable. As n_{KCl} is lowered further, surface effects govern the nanopore conductance. For a pore with a diameter of 10 nm and a value of the surface charge of 60 mC/m^2, as was found for SiO_2 nanochannels,[16] the crossover concentration is estimated at 120 mM. Indeed, the deviations from bulk behavior are found to occur near this concentration (Figure 2b).

Equation 1 now gives the conductance as a function of potassium chloride concentration (blue line in Figure 2b). In the high-salt regime, both the model and the experimental data show the linear bulk behavior. However, in the low-salt regime, the use of a constant surface-charge density results in a constant conductance. This clearly contradicts our experimentally observed behavior of a gradually decreasing conductance with decreasing KCl concentration.

However, the surface charge is not constant but should depend on the ion concentration. This follows from the chemical reactivity of the silicon dioxide surface given by

$$\text{SiOH} \rightleftarrows \text{SiO}^- + \text{H}^+ \qquad (2)$$

Assuming thermodynamic equilibrium, the concentration of H^+ ions near the surface is set by the local electrostatic potential. This potential drives the equilibrium of the chemical reaction and, hence, determines the amount of surface charge present. Behrends and Grier[27] derived a relationship between the potential at the no-slip plane (ζ potential) and the surface-charge density, σ, taking into account surface reactivity

$$\zeta(\sigma) = \frac{k_B T}{e} \ln\left(\frac{-\sigma}{e\Gamma + \sigma}\right) + \frac{k_B T \ln(10)}{e} (pK - pH) - \frac{\sigma}{C} \quad (3)$$

where $k_B T$ represents the thermal energy, Γ is the surface density of chargeable sites, pK is the equilibrium constant, and C is the capacitance of the Stern layer. An additional relationship between ζ and σ is given by the Grahame equation, which couples the electrostatic potential and the charge in the diffusive layer

$$\sigma(\zeta) = \frac{2\epsilon\epsilon_0 k_B T \kappa}{e} \sinh\left(\frac{e\zeta}{2k_B T}\right) \quad (4)$$

where $\epsilon\epsilon_0$ denotes the permittivity of the solution and κ^{-1} is the Debye screening length (equal to $\kappa^2 = 2e^2 n_{KCl}/k_B T \epsilon\epsilon_0$). Combining eqs 3 and 4 yields the surface charge as a function of the potassium chloride concentration. Recently, this model was used successfully by Van der Heyden et al. to model streaming currents in SiO_2 nanochannels as a function of salt concentration.[28] In the inset to Figure 2b, we plot $|\sigma|$ as a function of potassium chloride concentration using the parameters given in ref 28. When taking into account the chemical reactivity of the surface, the surface-charge density shows a monotonic decrease by more than 1 order of magnitude.

The varying surface charge obtained can be substituted into eq 1 to determine the salt-dependent conductance of a nanopore. The result is shown by the red line in Figure 2b. The dependence of the surface charge on the potassium chloride concentration, as predicted by the chemical equilibrium model, has a large impact on the nanopore conductance. As mentioned before, the conductance is dominated by bulk behavior in the high-salt regime. However, for potassium chloride concentrations below ~100 mM, the calculated conductance strongly deviates from both the bulk behavior and from the model that assumes a constant surface-charge density. The simple model presented here is remarkably consistent with the experimentally observed concentration dependence of the conductance. Upon adopting the parameters from literature and without the need of any fitting parameters, the model excellently describes the gradual decrease in conductance as the potassium chloride concentration is varied over the full range of salt concentrations.

DNA Translocation through Nanopores at Various Salt Concentrations. The salt dependence of DNA translocation is addressed with a model that considers two competing effects. On one hand, the conductance is decreased because of the volume that is occupied by the DNA.[29,30] In other words, the introduction of the DNA strand into the nanopore affects the bulk conductance by decreasing the number of charge carriers available for ionic transport. On the other hand, the counterions shielding the charge of the DNA backbone add a positive contribution to the ionic current. The DNA molecule introduces a cloud of mobile counterions into the pore, thereby increasing the number of charge carriers available for ionic transport.[21,22] Taking both effects into account, we can express the change in conductance, ΔG, due to DNA translocation as

$$\Delta G = \frac{1}{L_{pore}} \left(-\frac{\pi}{4} d_{DNA}^2 (\mu_K + \mu_{Cl}) n_{KCl}\, e + \mu_K^* q_{l,DNA}^* \right) \quad (5)$$

where d_{DNA} (2.2 nm) represents the diameter of the molecule, μ_K^* is the effective electrophoretic mobility of potassium ions moving along the DNA, and $q_{l,DNA}^*$ is the effective charge on the DNA per unit length, which is assumed to be constant. Because the left-hand term, expressing the change in bulk conductance, depends on n_{KCl}, we can expect a linear relationship for $\Delta G(n_{KCl})$ (as indeed observed experimentally, see Figure 4a) and, hence, a crossover point at which $\Delta G = 0$.

Free parameters $\mu_K^* q_{l,DNA}^*$ and L_{pore} in eq 5 can be obtained from the linear fit describing the data (Figure 4a). We obtain $\mu_K^* q_{l,DNA}^* = (2.09 \pm 0.06) \times 10^{-17}$ m/Ω and $L_{pore} = 34 \pm 2$ nm. The error denotes the standard deviation resulting from the fitting procedure. The value found for the length of a nanopore appears reasonable, considering the geometrical considerations sketched in Figure 1c.[31]

We can compare the effective electrophoretic mobility of potassium ions and the effective charge on the DNA per unit length to values reported in the literature. If we assume that μ_K^* equals the bulk ionic mobility, μ_K, then we can extract an effective charge on the DNA per unit length of $q_{l,DNA}^* = 0.58 \pm 0.02$ electron charges per basepair. This indicates a charge reduction of 71 ± 2% of the bare charge of $2e^-$ per basepair. Values reported in the literature for the effective charge on the DNA have been extracted previously from indirect measurements and vary widely.[32−34] With a direct measurement, the effective charge of the DNA was determined recently by Keyser et al.,[35] which yielded $q_{l,DNA}^* = 0.53 \pm 0.05$ electron charges per basepair, a value that compares well to the value reported here. Alternatively, one could assume a charge on the DNA of $2e^-$ per basepair and extract a reduced value for the effective mobility of the counterions of the DNA equal to $(2.22 \pm 0.06) \times 10^{-8}$ m^2/Vs.

The models developed above for G and conductance changes, ΔG, due to DNA translocation can be compared to the measured relative conductance change, $\Delta G/G$ (Figure 4b). Because of the limited salt range probed, the data do not discriminate well between models of constant or salt-dependent surface-charge density. We combine eqs 1, 3, 4, and 5 to calculate the expected $\Delta G/G$. This is shown in Figure 4b by the red line, using the same parameters as Van der Heyden et al.[28] and the product of $\mu_K^* q_{l,DNA}^*$ found above. The model gives a quite good description of the data.[36]

We attribute part of the variation between nanopores with similar diameters to a variation in surface charge. We conclude that the absolute change in conductance is the better parameter for characterizing translocations.

Conclusions. We have measured the ionic conductance through nanopores over a salt range of 6 orders of magnitude. A strong deviation from bulk behavior is found for potassium chloride concentrations lower than 100 mM. A much more gradual conductance decrease than expected from bulk models is measured for salt concentrations from 100 mM down to 1 μM. We show that the salt-dependent surface charge of 10-nm-diameter pores contributes significantly to the ionic current at these salt concentrations. A surface charge adapting according to the local chemical equilibrium is supported by the data.

The change in conductance during DNA translocation is observed to change from decreasing to increasing values as the potassium chloride concentration is lowered. In both cases, DNA folding and similar translocation times are recorded. We measured this change over a range of salt concentrations and determined the transition point where DNA translocation has no net effect on the ionic current. A simple model links the decreases in conductance to the volume occupied by the DNA, and the increases in conductance to the mobile counter charge of the DNA molecule. These experiments show that DNA translocation can be used to estimate the DNA volume and obtain a measure of its effective charge. This provides an extension of the Coulter counter principle and illustrates that nanopores may serve as a new tool to measure the dynamics and effective charge of polymers, proteins, and DNA−protein interactions.

Acknowledgment. We thank Kees Klein for his contributions to the experimental work and Frank van der Heyden, Derek Stein, and Serge Lemay for useful discussions. This work was funded by The Netherlands Organization for Scientific Research (NWO) and the Dutch Foundation for Fundamental Research on Matter (FOM).

References

(1) Kasianowicz, J. J.; Brandin, E.; Branton, D.; Deamer, D. W. *Proc. Natl. Acad. Sci. U.S.A.* **1996**, *93*, 13770.
(2) Song, L. Z.; Hobaugh, M. R.; Shustak, C.; Cheley, S.; Bayley, H.; Gouaux, J. E. *Science* **1996**, *274*, 1859.
(3) Akeson, M.; Branton, D.; Kasianowicz, J. J.; Brandin, E.; Deamer, D. W. *Biophys. J.* **1999**, *77*, 3227.
(4) Meller, A.; Nivon, L.; Brandin, E.; Golovchenko, J.; Branton, D. *Proc. Natl. Acad. Sci. U.S.A.* **2000**, *97*, 1079.
(5) Vercoutere, W.; Winters-Hilt, S.; Olsen, H.; Deamer, D.; Haussler, D.; Akeson, M. *Nat. Biotechnol.* **2001**, *19*, 248.
(6) Howorka, S.; Movileanu, L.; Braha, O.; Bayley, H. *Proc. Natl. Acad. Sci. U.S.A.* **2001**, *98*, 12996.
(7) Li, J.; Stein, D.; McMullan, C.; Branton, D.; Aziz, M. J.; Golovchenko, J. A. *Nature* **2001**, *412*, 166.
(8) Storm, A. J.; Chen, J. H.; Ling, X. S.; Zandbergen, H. W.; Dekker, C. *Nat. Mater.* **2003**, *2*, 537.
(9) Keyser, U. F.; Krapf, D.; Koeleman, B. N.; Smeets, R. M. M.; Dekker, N. H.; Dekker, C. *Nano Lett.* **2005**, *5*, 2253.
(10) Storm, A. J.; Storm, C.; Chen, J. H.; Zandbergen, H.; Joanny, J. F.; Dekker, C. *Nano Lett.* **2005**, *5*, 1193.
(11) Fologea, D.; Uplinger, J.; Thomas, B.; McNabb, D. S.; Li, J. L. *Nano Lett.* **2005**, *5*, 1734.
(12) Li, J. L.; Gershow, M.; Stein, D.; Brandin, E.; Golovchenko, J. A. *Nat. Mater.* **2003**, *2*, 611.
(13) Storm, A. J.; Chen, J. H.; Zandbergen, H. W.; Dekker, C. *Phys. Rev. E* **2005**, *71*, 051903.
(14) Heng, J. B.; Ho, C.; Kim, T.; Timp, R.; Aksimentiev, A.; Grinkova, Y. V.; Sligar, S.; Schulten, K.; Timp, G. *Biophys. J.* **2004**, *87*, 2905.
(15) Bezrukov, S. M. *J. Membr. Biol.* **2000**, *174*, 1.
(16) Stein, D.; Kruithof, M.; Dekker, C. *Phys. Rev. Lett.* **2004**, *93*, 035901.
(17) Schoch, R. B.; Renaud, P. *Appl. Phys. Lett.* **2005**, *86*, 253111.
(18) Karnik, R.; Castelino, K.; Fan, R.; Yang, P.; Majumdar, A. *Nano Lett.* **2005**, *5*, 1638.
(19) Ho, C.; Qiao, R.; Heng, J. B.; Chatterjee, A.; Timp, R. J.; Aluru, N. R.; Timp, G. *Proc. Natl. Acad. Sci. U.S.A.* **2005**, *102*, 10445.
(20) Siwy, Z.; Kosinska, I. D.; Fulinski, A.; Martin, C. R. *Phys. Rev. Lett.* **2005**, *94*, 048102.
(21) Chang, H.; Kosari, F.; Andreadakis, G.; Alam, M. A.; Vasmatzis, G.; Bashir, R. *Nano Lett.* **2004**, *4*, 1551.
(22) Fan, R.; Karnik, R.; Yue, M.; Li, D. Y.; Majumdar, A.; Yang, P. D. *Nano Lett.* **2005**, *5*, 1633.
(23) Wu, M. Y.; Krapf, D.; Zandbergen, M.; Zandbergen, H.; Batson, P. E. *Appl. Phys. Lett.* **2005**, *87*, 113106.
(24) The most probable translocation time is the time associated with the peak in the distribution. The error that is quoted is dominated by temperature variations in the setup. A variation of about 3 degrees leads to an estimated error of 10% (cf. ref 11).
(25) At a KCl concentration of 300 mM, the traces occasionally show events that were composed of a first part of current blockades and a second part of enhancements. Because the current enhancements dominated the behavior and no current blockades events were recorded, only the current enhancements were analyzed.
(26) Lide, D. R. *CRC Handbook of Chemistry and Physics*., 85th ed.; internet version, 2005.
(27) Behrens, S. H.; Grier, D. G. *J. Chem. Phys.* **2001**, *115*, 6716.
(28) van der Heyden, F. H. J.; Stein, D.; Dekker, C. *Phys. Rev. Lett.* **2005**, *95*, 116104.
(29) Deamer, D. W.; Olsen, H.; Akeson, M. A.; Kasianowicz, J. J. Mechanism of ionic current blockades during polymer transport through pores of nanometer dimensions. In *Structure and Dynamics of Confined Polymers*; Kasianowicz, J. J., Kellermayer, M. S. Z., Deamer, D. W., Eds.; Kluwer Academic Publishers: Dordrecht, The Netherlands, 2002; p 165.
(30) Rabin, Y.; Tanaka, M. *Phys. Rev. Lett.* **2005**, *94*, 148103.
(31) The value found here was also used for calculations on the salt dependence of the nanopore conductance as discussed in relation to Figure 2.
(32) Manning, G. S. *Q. Rev. Biophys.* **1978**, *11*, 179.
(33) Schellman, J. A.; Stigter, D. *Biopolymers* **1977**, *16*, 1415.
(34) Stellwagen, E.; Stellwagen, N. C. *Biophys. J.* **2003**, *84*, 1855.
(35) Keyser, U. F.; Koeleman, B. N.; Krapf, D.; Smeets, R. M. M.; Lemay, S. G.; Dekker, N. H.; Dekker, C., submitted for publication.
(36) The one data point at 100 mM, which has a lower value of the relative change in conductance, was measured with a 20-nm-diameter pore, whereas the red line was calculated for a pore diameter of 10 nm.

NL052107W